Reconstruction and dislocation network formation of the (111) surface of the ordered alloy Pt$_3$Sn

J. Kuntze, S. Speller, and W. Heiland

Universität Osnabrück, FB Physik, D-49069 Osnabrück, Germany

A. Atrei

Dipartimento di Scienze e Tecnologie Chimiche e dei Biosistemi, Università di Siena, 53100 Siena, Italy

I. Spolveri and U. Bardi

Dipartimento di Chimica, Università di Firenze, 50121 Firenze, Italy

A Scanning tunneling microscopy study of the ordered alloy Pt$_3$Sn is presented. The (111) surface shows a bulk terminated $p(2\times2)$ structure or a $(\sqrt{3}\times\sqrt{3})$ $R30°$ reconstruction, depending on preparation conditions. In addition, the reconstructed surface exhibits a mesoscopic honeycomb network. The network indicates the presence of subsurface dislocations, which are induced by a tin depletion due to preferential sputtering. On the $p(2\times2)$ structure small islands with uniform size are found, which are attributed to segregated tin. [S0163-1829(98)50948-4]

The study of the surface properties of the Pt-Sn binary system has been prompted by its interest in heterogeneous catalysis.[1] Early theoretical studies on the surface composition were carried out by Sachtler and Van Santen[2] and in recent years the surface of the Pt-Sn systems has been extensively investigated by various surface science techniques.[3] All studies have evidenced a strong tendency of this system to form ordered surface phases.

The ordered phases forming on the (111) face of Pt$_3$Sn have been structurally characterized in previous works by crystallographic low-energy electron diffraction (LEED),[4] x-ray photoelectron diffraction (XPD),[5] quantitative low energy ion scattering (LEIS), and LEED spot profile analysis.[6] Here we use scanning tunneling microscopy (STM) to examine the Pt$_3$Sn(111) surface. The atomically resolved images of the observed structures [$p(2\times2)$ bulk truncation and $(\sqrt{3}\times\sqrt{3})$ $R30°$ reconstruction] are in agreement with the previous crystallographic studies. Both the $p(2\times2)$ and the $(\sqrt{3}\times\sqrt{3})$ $R30°$ phase are accompanied by additional features: On the $(\sqrt{3}\times\sqrt{3})$ $R30°$ phase a mesoscopic, nearly hexagonal ''honeycomb'' network is observed. We attribute this network to the presence of ''buried'' dislocations, in turn generated by the lattice mismatch caused by tin depletion in the subsurface region, which has been shown to stabilize the $(\sqrt{3}\times\sqrt{3})$ $R30°$ structure.[5,7] On the $p(2\times2)$ domains small islands of uniform size are found, which probably consist of tin.

All measurements were carried out in an ultrahigh-vacuum system equipped with a scanning tunneling microscope (Omicron STM-1) operating at room temperature in the constant current mode. The STM has been calibrated using the atomically resolved Si(111)(7$\times$7) and Pt(110)(1$\times$2) surfaces. The system is also equipped with LEED (low-energy electron diffraction) and AES (Auger electron spectroscopy). The sample surface was prepared by cycles of sputtering using 500-eV Ar$^+$ ions followed by annealing. Temperatures were measured with a pyrometer and a thermocouple fixed at the manipulator head near the sample.

In agreement with previous studies,[5,6] we observed by AES that the ion bombardment causes a depletion of tin in the surface region. Annealing to 600 K does not significantly change the AES Pt/Sn ratio, but after annealing at 1000 K the Sn concentration strongly increases indicating the gradual restoring of the bulk composition. Quantitative evaluations of the Pt(241 eV) and the Sn(432) dN/dE signals using sensitivity factors reported in Ref. 8 are compatible with a 3:1 Pt/Sn atomic ratio after high-temperature annealing.

After sputtering and annealing, the LEED pattern shows both the $(\sqrt{3}\times\sqrt{3})$ $R30°$ and the $p(2\times2)$ periodicities, in agreement with previous studies.[4,5,9,10] For low annealing temperatures the $(\sqrt{3}\times\sqrt{3})$ $R30°$ phase is dominant, conversely the $p(2\times2)$ phase becomes dominant for high annealing temperatures.

$(\sqrt{3}\times\sqrt{3})$ $R30°$ *structure.* STM images (Fig. 1) taken after annealing to 600 K show a mesoscopic honeycomb network structure. The atomically resolved STM images clearly show that the meshes of the network are not different domains of the $(\sqrt{3}\times\sqrt{3})$ $R30°$ structure. A domain boundary also visible in the figure is easily distinguishable from the walls of the network. The height of the walls is 0.6–0.7 Å, and the mean width of these features is ~150 Å. The imaging of the network is independent of tunneling parameters, and hence cannot be an artifact due to electronic effects. A simple moiré pattern can also be ruled out as an explanation, since the observed network is not perfectly hexagonal, especially after annealing at temperatures lower than 600 K. Furthermore the network is not due to a mere surface effect, i.e., restricted to the topmost layer only, since it is undistorted by atomic steps (not shown in the figures presented here).

The atomically resolved structure is shown in Fig. 2. The data available from a previous crystallographic LEED study[5] provide a structural model also shown in Fig. 2. Taking into account also the results of the quantitative LEIS measurements[6] (i.e., a surface concentration of 75 at. % Pt
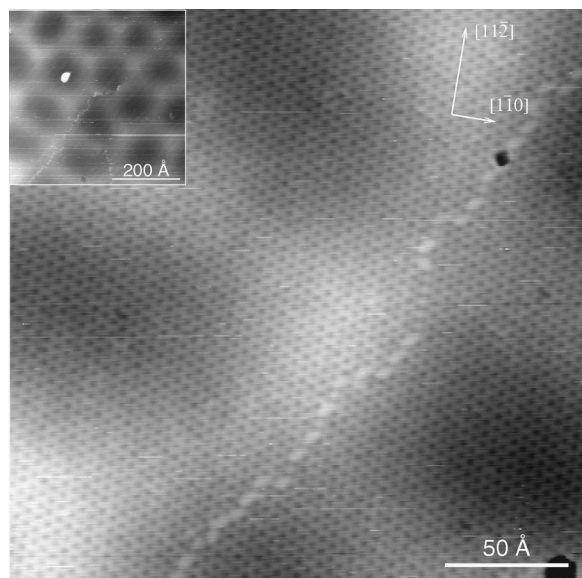
FIG. 1. STM images of the $(\sqrt{3} \times \sqrt{3}) R30°$ structure taken after annealing to 600 K, $U_t = 0.1$ V, $I_t = 0.5$ nA. The inset shows a $(530 \text{ Å})^2$ terrace with the quasihexagonal honeycomb network. The main image is a close-up view of the inset's lower left region, size $(236 \text{ Å})^2$. Both the atomic structure and the height modulation due to the honeycomb network are visible. The irregular line running from the lower left to the upper right corner is a domain wall separating two different $(\sqrt{3} \times \sqrt{3}) R30°$ domains. It shows a defect in the upper right region.

and 25 at. % Sn), the attribution of the features observed with STM is unambiguous: the bright regions (high tunnel current) can be identified as Pt atoms and the dark regions (low tunnel current) as Sn atoms. This is independent of tunneling parameters in the tested range of $\pm(0.1-0.9)$ V for the gap voltage and $(0.5-3.0)$ nA for the tunneling current. Calculations of the density of states for the Pt_3Sn alloy indicate a band gap at the Sn sites near the Fermi edge,[11] which explains the contrast observed by STM.

The honeycomb network is attributed to misfit dislocations in deeper layers, which are produced by preferential sputtering of tin. XPD measurements[5] indicate that the subsurface region is strongly depleted in tin, in agreement with our AES measurements, whereas the topmost monolayer is enriched in tin according to LEIS (Refs. 6, 9, and 10) and
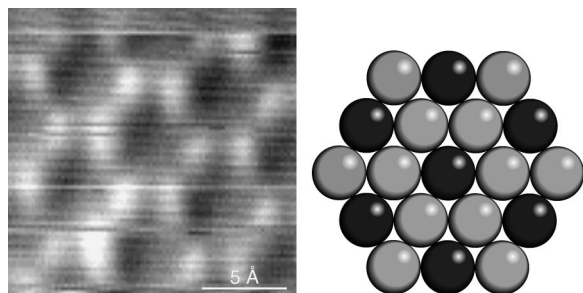

FIG. 2. $(17 \text{ Å})^2$ high-resolution image $(U_t = 0.9$ V, $I_t = 1.0$ nA$)$ and hard-sphere model of the $(\sqrt{3} \times \sqrt{3}) R30°$ structure, as derived by crystallographic LEED (Ref. 5). Due to some drift the image is slightly elongated in the vertical direction. Pt corresponds to regions of high tunnel current (bright areas), Sn corresponds to regions of low tunnel current (dark areas).

LEED studies.[4] Due to the different tin concentration the lattice parameter of the subsurface region should be close to the lattice constant of pure Pt $(a_{Pt} = 3.92$ Å$)$, slightly less than the bulk value of Pt_3Sn $(a_{Pt_3Sn} = 4.00$ Å$)$,[4] leading to tensile stress in the Sn-depleted subsurface layers, which is relieved by the dislocations. On the other hand, the Sn-enriched topmost layer may be compressively strained. This stress may be accommodated by buckling of the tin atoms, which has been found by crystallographic LEED.[4,5]

Formation of misfit dislocations is a well-known mechanism for strain relief in heteroepitaxial films,[12–15] but the substitutionally disordered Pt_xNi_{1-x} system is the only bulk alloy for which misfit dislocations have been reported.[16,17] The $Pt_3Sn(111)$ surface is the first ordered bulk alloy for which misfit dislocations due to preferential sputtering have been found.

Since we observed no dislocations reaching the surface, the Burgers vector of the buried dislocations can only be determined indirectly: the walls of the network are aligned along the $\langle 112 \rangle$ directions, thus the corresponding Burgers vector would be $\frac{1}{2}\langle 110 \rangle$, parallel to the surface. The alignment of the network walls is observed mainly after annealing to temperatures higher than 600 K, whereas at lower annealing temperatures the network appears distorted.

The depth of the dislocation cores can be estimated via the cross section of the walls of the dislocation network, as has been shown in Ref. 12 for dislocation networks on thin films. Since the half-width of a section profile across a wall is $\sim30-40$ Å in our case, this estimation yields a depth of roughly 15 atomic layers for the dislocations. The observed depletion in Sn should therefore be restricted to this region, which is compatible with the previous XPD results.[5]

p(2×2) *structure.* Upon annealing to 1000 K for 20–30 min the terraces grow larger and the surface is now dominated by $p(2\times2)$ domains. They can be identified on large-scale STM images (Fig. 3) by clusters or islands and a disappearance of the honeycomb network, which can also be seen on high-resolution images of the boundary region between the $p(2\times2)$ and the $(\sqrt{3} \times \sqrt{3}) R30°$ domains (Fig. 4). The atomic structure is in agreement with previous LEED studies.[4] As can be seen from a section profile in Fig. 4, the clusters are 1.8–2.3 Å high, in good agreement with atomic step heights. Since single atoms would probably appear more shallow, the features may indeed be small islands of at least three atoms, since they are round shaped. The islands show no structure, therefore it is not possible to count the atoms. For Pb atoms on Cu(111) (Ref. 18) an enlarged size of single adatoms has been reported, but the Pb atoms still appeared much smaller than the islands in the present case. The islands are only weakly bound, as they often are dragged over the surface by the tip, which can also be seen in the lower left region in Fig. 4.

From Fig. 3 the atomic concentration of the adatoms at the surface can be estimated to be approximately 1 at. % (assuming islands of three atoms). Recent quantitative LEIS measurements have indicated a slight but significant increase in the Sn concentration in the topmost layer,[6] and earlier studies[9,10] indicated a rise in the Sn/Pt ratio upon grazing incidence, which was attributed to a Sn buckling of 0.2 Å, in agreement with LEED.[4] The increased Sn/Pt ratio in LEIS could also (at least partly) be due to Sn adatoms.
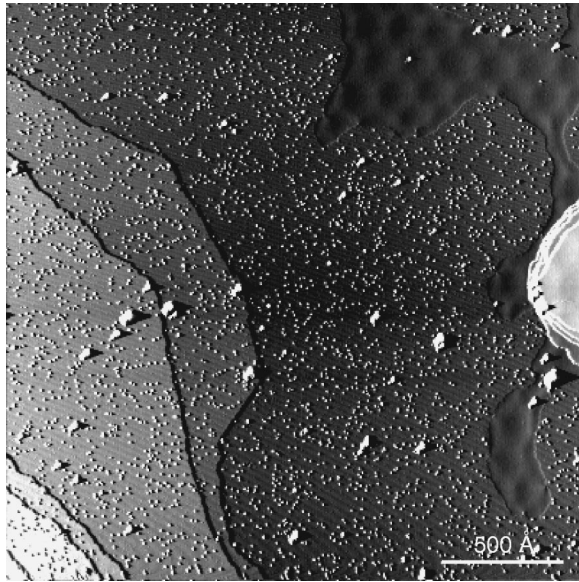
FIG. 3. STM image of the mixed $p(2\times2)$ and $(\sqrt{3}\times\sqrt{3})$ $R30°$ structure taken after annealing to 1000 K, size $(2400 \text{ Å})^2$, $U_t=0.9$ V, $I_t=1.0$ nA. The image has been differentiated to enhance contrast. The small adatom islands mark the $p(2\times2)$ domains (compare Fig. 4), whereas in the upper right corner $(\sqrt{3}\times\sqrt{3})$ $R30°$ areas with the honeycomb network remain. The larger clusters may be due to residual contaminants, below the AES detection limit.

Since the bulk-truncated $p(2\times2)$ structure develops via the Sn-enriched $(\sqrt{3}\times\sqrt{3})$ $R30°$ phase, the Sn atoms in excess have either to be incorporated into subsurface layers or pushed out of the surface to form adatoms. In the latter case, the expected adatom concentration would amount to 1/12 ML, i.e., ~8 at. %, which seems higher than the observed concentration. Therefore incorporation into subsurface layers may be the main mechanism to reduce the Sn concentration in the topmost layer.

As can be seen in Fig. 4, the boundary between the $p(2\times2)$ and the $(\sqrt{3}\times\sqrt{3})$ $R30°$ domains are very sharp. The nucleation of the $p(2\times2)$ domains starts in the center of the meshes forming the honeycomb network. This has been repeatedly observed after annealing to 800 K, but since the transition is fast, it is easily missed if heating too long or at a too high temperature. The rapid transformation of the $(\sqrt{3}\times\sqrt{3})$ $R30°$ phase to the $p(2\times2)$ phase is in agreement with SPALEED studies[6] which report a very fast growth of the $p(2\times2)$ domains, once they nucleate.

STM confirms the atomic model for the $(\sqrt{3}\times\sqrt{3})$ $R30°$ reconstruction and the $p(2\times2)$ bulk truncation of the $Pt_3Sn(111)$ surface proposed by LEED and XPD. Our AES results also confirm a depletion of tin in the surface region after sputtering found by XPD. This depletion leads to misfit
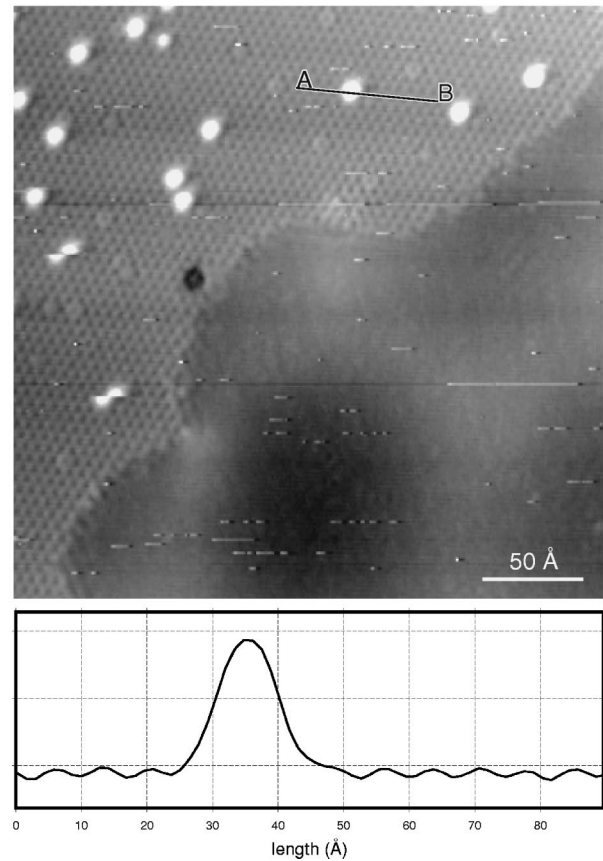

FIG. 4. STM image of the boundary region of a $p(2\times2)$ (upper left half) and a $(\sqrt{3}\times\sqrt{3})$ $R30°$ domain (lower right half, not atomically resolved), size $(293 \text{ Å})^2$, $U_t=0.9$ V, $I_t=1.0$ nA. The gray scale has been restricted to the flat surface, to enhance visibility of the $p(2\times2)$ atomic structure. The height of the adatom feature on the $p(2\times2)$ region equals approximately an atomic step (section profile). Note the two adatom features in the left region, which have been moved by the tip.

dislocations in the subsurface region, which causes a mesoscopic honeycomb network on the $(\sqrt{3}\times\sqrt{3})$ $R30°$ domains. The mean width of these features is ~150 Å, with a height of 0.6–0.7 Å. A simple estimation yields a depth of the dislocation cores of roughly 15 atomic layers. Upon annealing to temperatures ≥800 K $p(2\times2)$ domains prevail, on which the honeycomb-network is lifted. On these domains adatom-islands are found, which may consist of Sn atoms. The observed STM contrast between Pt and Sn can be explained by a band gap for Sn at the Fermi edge.

[1] R. Bouwman, L. H. Toneman, and A. A. Holscher, Surf. Sci. **35**, 8 (1973).

[2] R. A. Van Santen and W. M. H. Sachtler, J. Catal. **33**, 202 (1974).

[3] U. Bardi, Rep. Prog. Phys. **57**, 939 (1994).

[4] A. Atrei, U. Bardi, G. Rovida, M. Torrini, and E. Zanazzi, Phys. Rev. B **46**, 1649 (1992).

[5] A. Atrei, U. Bardi, M. Torrini, E. Zanazzi, G. Rovida, H. Kasamura, and M. Kudo, Condens. Matter Phys. **5**, L207 (1993).

[6] W. C. A. N. Ceelen, A. W. Denier van der Gon, M. A. Reijme, H. H. Brongersma, I. Spolveri, A. Atrei, and U. Bardi, Surf. Sci. **406**, 264 (1998).

[7] C. Gallis, B. Legrand, and G. Tréglia, Surf. Sci. **377**, 1033 (1997).

[8] *Handbook of Auger Electron Spectroscopy*, edited by C. L. Hedberg (Physical Electronics, Inc., Eden Prairie, MN, 1995).

[9] A. N. Haner, P. N. Ross, and U. Bardi, Catal. Lett. **8**, 1 (1991).

[10] A. N. Haner, P. N. Ross, and U. Bardi, Surf. Sci. **249**, 15 (1991).

[11] J. Kuntze, S. Speller, A. Postnikov, and W. Heiland (unpublished).

[12] R. Stalder, H. Sirringhaus, N. Onda, and H. von Känel, Appl. Phys. Lett. **59**, 1960 (1991).

[13] H. Bethge, D. Heuer, Ch. Jensen, K. Reshöft, and U. Köhler, Surf. Sci. **331-333**, 878 (1995).

[14] J. G. Belk, J. L. Sudijono, H. Yamaguchi, X. M. Zhang, D. W. Pashley, C. F. McConville, T. S. Jones, and B. A. Joyce, J. Vac. Sci. Technol. A **15**, 915 (1997).

[15] H. Brune, Surf. Sci. Rep. **31**, 121 (1998).

[16] M. Schmid, A. Biedermann, H. Stadler, C. Slama, and P. Varga, Appl. Phys. A: Solids Surf. **55**, 468 (1992).

[17] M. Schmid, A. Biedermann, C. Slama, H. Stadler, P. Weigand, and P. Varga, Nucl. Instrum. Methods Phys. Res. B **82**, 259 (1993).

[18] C. Nagl, O. Haller, E. Platzgummer, M. Schmid, and P. Varga, Surf. Sci. **321**, 237 (1995).